fluids

MDPI

Article

Boundary Layer Flow and Heat Transfer of FMWCNT/Water Nanofluids over a Flat Plate

Mohammad Reza Safaei [1], Goodarz Ahmadi [2,*], Mohammad Shahab Goodarzi [3], Amin Kamyar [4] and S. N. Kazi [1]

1 Department of Mechanical Engineering, Faculty of Engineering, University of Malaya, Kuala Lumpur 50603, Malaysia; cfd_safaei@um.edu.my (M.R.S.); salimnewaz@um.edu.my (S.N.K.)
2 Department of Mechanical and Aeronautical Engineering, Clarkson University, Potsdam, NY 13699-5725, USA
3 Department of Mechanical Engineering, Mashhad Branch, Islamic Azad University, Mashhad 9187147578, Iran; shahabg25269@yahoo.com
4 School of Mechanical and Mining Engineering, The University of Queensland, Brisbane, QLD 4072, Australia; amn_kam@yahoo.com
* Correspondence: gahmadi@clarkson.edu; Tel.: +1-315-268-2322

Academic Editor: Bekir S. Yilbas
Received: 16 March 2016; Accepted: 15 September 2016; Published: 26 September 2016

Abstract: In the present study, the heat transfer and flow of water/FMWCNT (functionalized multi-walled carbon nanotube) nanofluids over a flat plate was investigated using a finite volume method. Simulations were performed for velocity ranging from 0.17 mm/s to 1.7 mm/s under laminar regime and nanotube concentrations up to 0.2%. The 2-D governing equations were solved using an in-house FORTRAN code. For a specific free stream velocity, the presented results showed that increasing the weight percentage of nanotubes increased the Nusselt number. However, an increase in the solid weight percentage had a negligible effect on the wall shear stress. The results also indicated that increasing the free stream velocity for all cases leads to thinner boundary layer thickness, while increasing the FMWCNT concentration causes an increase in the boundary layer thickness.

Keywords: water/FMWCNT nanofluid; flat plate; boundary layer flow

PACS: 44; 47

1. Introduction

Heat transfer fluids (HTFs) with enhanced thermal performance have attracted considerable attention in a wide range of industries including vehicle manufacturing, transportation, electronics and air conditioning. Effective thermal management techniques are needed for cooling various kinds of high heat flux devices. Common HTFs such as water, ethylene glycol, and industrial oils have limited heat transfer abilities because of their low thermal conductivity. In contrast, metals have significantly higher thermal conductivities [1]. Hence, it is of considerable interest to develop and use suspensions as heat transfer fluids which flow readily but have an enhanced thermal conductivity close to metals [2]. Before the advancement of manufacture techniques for synthesis of nano-sized particles, some studies were performed on the effects of adding millimeter- or micrometer-sized particles to a base fluid [3]. Though inclusion of these types of particles generated fluids with enhanced thermal conductivity, they caused other issues like sedimentation, producing large pressure drops, clogging flow passages, and creating premature wear on duct walls and components [4]. Because nano-sized particles are extremely small, approaching the size of large molecules in their lower limit, their gravitational sedimentation is negligible and the potential for causing clogging and/or wear is very low [5]. Thus, nanofluids are inherently superior HTFs compared to the microfluids [6].

In recent years, most studies have been focused on determining the thermal conductivity of nanofluids and not much attention has been given to finding the heat transfer coefficient for convective heat transfer of nanofluids [7]. Recently, studies of forced convection of nanofluids over a flat plate were reported in the literature [8–11]. In these works, typically the method of similarity solution was used. In the present study, laminar forced convection over a horizontal flat was analyzed using the full momentum (Navier-Stokes) equation. The influences of inlet velocity and solid volume concentration as well as variable thermophysical properties of nanotubes on the flow and thermal field were studied. For this purpose, the experimental data from the literature were extracted and curve fittings were done on the data to find the appropriate thermophysical properties equations for the nanofluid. Special attention was given to the laminar forced convection of nanofluids made of suspension of functionalized multi-walled carbon nanotube (FMWCNT) in water with different weight percentages. The variations of velocity, temperature, wall shear stress as well as the Nusselt number along the plate were also evaluated and discussed. The effect of buoyancy effect was slowly included but was found to be small. The result of the present study may find applications for coolant fluids in solar collectors and electronic devices [12].

2. Governing Equations for Nanofluids Heat Transfer

To simulate laminar forced convection of nanofluid over a flat plate, the coupled continuity, X and Y momentum and energy equations are solved. The corresponding governing equations are given as [13–15]:

$$\frac{\partial u}{\partial x} + \frac{\partial v}{\partial y} = 0 \tag{1}$$

$$\begin{array}{c} u\frac{\partial u}{\partial x} + v\frac{\partial u}{\partial y} = -\frac{\partial P}{\partial x} + \frac{\partial}{\partial x}\left(\frac{\mu}{\rho}\frac{\partial u}{\partial x}\right) + \frac{\partial}{\partial y}\left(\frac{\mu}{\rho}\frac{\partial u}{\partial y}\right) \\ u\frac{\partial v}{\partial x} + v\frac{\partial v}{\partial y} = \frac{\partial}{\partial x}\left(\frac{\mu}{\rho}\frac{\partial v}{\partial x}\right) + \frac{\partial}{\partial y}\left(\frac{\mu}{\rho}\frac{\partial v}{\partial y}\right) + g\beta(T - T_\infty) \end{array} \tag{2}$$

$$u\frac{\partial T}{\partial x} + v\frac{\partial T}{\partial y} = \frac{\partial}{\partial x}\left(\frac{k}{\rho C_p}\frac{\partial T}{\partial x}\right) + \frac{\partial}{\partial y}\left(\frac{k}{\rho C_p}\frac{\partial T}{\partial y}\right) \tag{3}$$

where u, v are component of velocity vectors, T is the temperature, P is pressure, ρ is the fluid density, μ is the effective viscosity of nanofuid, C_p is the heat capacity, β is the coefficient of thermal expansion, and k is the effective heat conductivity of nanofluid.

The local Nusselt number and the heat transfer coefficient along the wall can be obtained from the following relation [16],

$$Nu_x = \frac{k_{nf}}{k_{bf}}\left(\frac{\partial T}{\partial Y}\right)_{Y=0} \tag{4}$$

3. Nanofluid Properties

The thermophysical properties of water/functionalized multi-walled carbon nanotube (FMWCNT) nanofluids were experimentally evaluated by Amrollahi, et al. [17], a summary of which is reported in Table 1. These values were used in the present investigation. Two regressions on the experimental data for evaluating the effective thermal conductivity and effective viscosity of the nanofluid were performed. Accordingly, for 0 wt. % $\leq \phi \leq$ 0.25 wt. % and 20 °C $\leq T \leq$ 33 °C,

$$\mu = 0.00139 + (0.000189\phi) + (-1.80 \times 10^{-5}T) \tag{5}$$

$$k = 0.55633 + (0.453111\phi) + (6.61 \times 10^{-5}T^2) \tag{6}$$

For solid weight percentage, less than 0.25 wt. %, the measured heat capacity of nanofluids was found to be the same as that of water [17].

Table 1. Experimental data of thermophysical properties of the base fluid and nanofluids [17,18].

Wt. % FMWCNT/Water	Density ($kg \cdot m^{-3}$)	Viscosity ($kg \cdot m^{-1} \cdot s^{-1}$)			Thermal Conductivity ($W \cdot m^{-1} \cdot K^{-1}$)		
		20 °C	27 °C	33 °C	20 °C	27 °C	33 °C
0	995.8 (26.6 °C)	0.000980	0.000860	0.000765	0.59	0.61	0.62
0.1	1003 (23.4 °C)	0.000998	0.000881	0.000781	0.62	0.64	0.66
0.2	1006 (23.1 °C)	0.00103	0.000901	0.000790	0.67	0.69	0.71

4. Boundary Conditions

Figure 1 illustrates the schematic drawing of the nanofluid flow over the flat plate which is analyzed in the present study. On surface of the plate, no-slip boundary conditions were used. The effect of buoyancy force was also included in the analysis. The gauge pressure was set as the boundary condition of upper and right sides of the flow domain. This boundary condition lead to more accurate results, but makes the solution convergence harder and more time consuming [19]. The plate has been considered sufficiently wide to avoid any variation in flow properties in spanwise direction. The inlet fluid temperature and plate temperature were fixed, respectively, at 293 K and 306 K. The velocity of the HTF was varied from 0.00017 m/s to 0.0017 m/s. Simulations were performed for a mixture of distilled water and FMWCNT with different weight percentages.

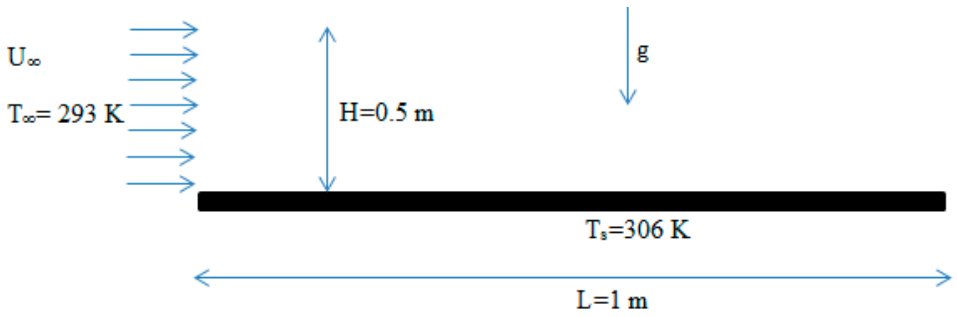

Figure 1. Schematic drawing of the computational configuration.

5. Numerical Procedure

In the present study, an in-house FORTRAN code based on Finite Volume Method [20] was developed and used to solve the governing equations. The finite volume method is a specific case of the residual weighting method. In this approach, the computational field is divided into a number of control volumes in such a way that each computational node is surrounded by a control volume and the control volumes have no common parts. Then, the governing equations are integrated over each control volume. The results are discretization equations that are used in the simulation. Finally, a line by line tridiagonal matrix algorithm (TDMA) method is utilized to solve the discretized algebraic governing equations over the solution domain. The main advantage of this method is high accuracy even when a relatively low number of nodes are used. Additional details of this computational method were reported in [21,22].

All the equation terms were discretized by the method of second order upwind [15], and the pressure and velocity equations were coupled using the SIMPLE algorithm [23]. The convergence of solution was achieved when the residuals of all the equations fell below 10^{-6} [24].

6. Validation

In order to verify the accuracy of present simulations, the computational model predictions for the laminar flow of pure water for range of velocity $0.00017 \leq U \leq 0.0017$ m/s over a flat plate were compared with the exact solution. Here the range of Reynolds number was $172.74 \leq Re \leq 1727.41$. For different inlet velocities, the computed local wall shear stresses and Nusselt numbers at the end of

the plate are evaluated and the results are listed in Table 2. The prediction of the exact solutions in the absence of natural convection are given as [25]:

$$C_{f,x} = \frac{0.664}{\sqrt{\mathrm{Re}_x}} \tag{7}$$

$$\tau_w(x) = 0.5 C_{f,x} \rho U_\infty^2 \tag{8}$$

$$Nu = 0.332 \mathrm{Pr}^{\frac{1}{3}} \mathrm{Re}_x^{\frac{1}{2}} \tag{9}$$

Table 2. Comparison of predicted wall shear stress with the exact solution.

U (m/s)	Exact Solution			Present Study	
	C_f	τ (Pa)	Nu	τ (Pa)	Nu
0.00017	0.051	7.37×10^{-7}	8.326	7.79×10^{-7}	8.798
0.001	0.021	1.05×10^{-5}	20.193	1.12×10^{-5}	21.538
0.0017	0.016	2.30×10^{-5}	26.328	2.45×10^{-5}	27.998

From Table 2, it is seen that the present numerical results are in reasonable agreement with the results of exact solution with an error of about 6.5%. Therefore, the current numerical procedure can be used for simulating the laminar flow of nanofluids at low solid concentration over a flat plate.

7. Grid Independence

A non-uniform, structured grid was used for the discretization of the studied domain. A greater number of grids were used near the inlet, outlet, and walls, where thermofluidic gradients were high. Different mesh distributions were studied to assure that the solution is mesh independent. Table 3 shows the predicted local friction coefficient for different grid sizes. It is seen that, for grids larger than 110×55, the variation in the coefficient of friction is negligibly small. Therefore, the 110×55 grid was used for all the subsequent studies.

Table 3. Grid independence tests for the present study: U = 0.001 m/s and distilled water.

Local Coefficient of Friction	Number of Grids
0.02342	50×25
0.02286	75×40
0.02252	100×50
0.02249	110×55
0.02247	125×65
0.02245	150×75

8. Results and Discussion

Different solid weight percentages and three free stream velocities for flow over the flat plate were used in the present simulations. The fluid flow and thermal field characteristics as well as Nusselt number for water/FMWCNT nanofluid were also studied in details. Particular attention was given to the effect of variations of nanotube weight percentage and free stream velocity on the convective heat transfer properties.

Figure 2 illustrates the temperature profiles at X/L = 0.5, for different free stream velocities and nanotube weight percentages. Figure 2b shows an enlarged section of the profile for clarity. The presented results show that, for all cases, the temperature stays constant except in the thermal boundary layer region, where the temperature changes from 306 K at the surface of the plate to 293 K. It is also seen that for all cases, the thermal boundary layer thickness increases as the weight

percentages increases or velocity decreases. The effect of variation in the velocity, however, is much larger than that of the changes in the solid concentration in the range of 0 to 0.2 wt. %. This is perhaps because of the very small solid weight percentage used. The highest thermal boundary layer value was seen at 0.2 wt. % and free stream velocity = 0.17 mm/s.

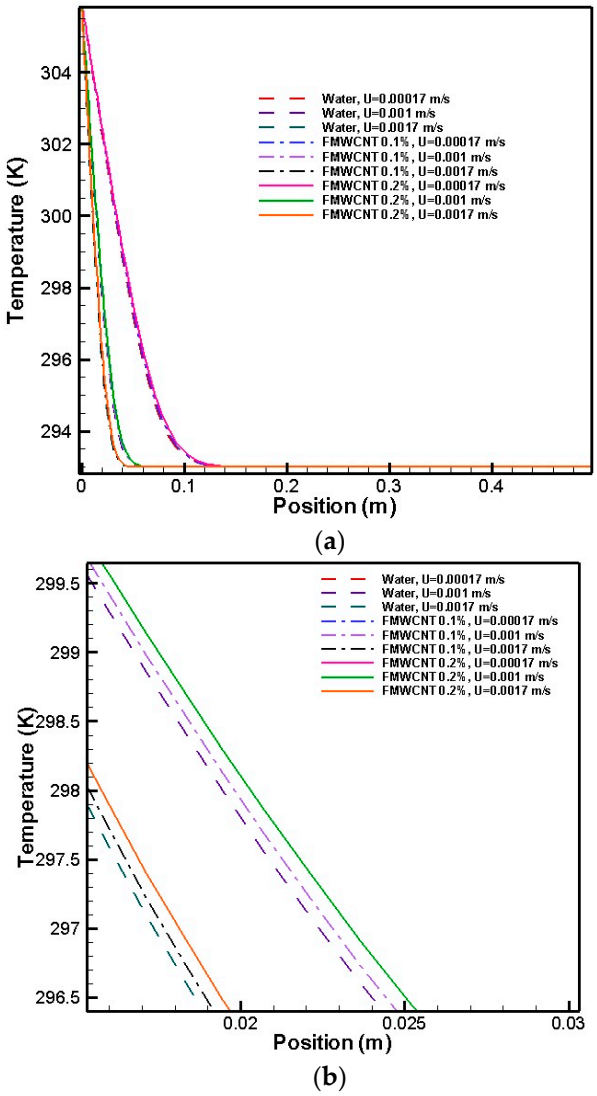

Figure 2. Temperature profiles versus distance from the plate at x = 0.5 m for different free stream velocities and nanotube weight percentages. (**a**) Full profile; (**b**) Enlarged segment near the plate.

Figures 3 and 4 show the effects of different values of free stream velocity and nanotube weight percentage on the velocity variation and boundary layer formation. In Figure 3, the velocity profiles across the vertical centreline of the flat plate at X/L = 0.5 are shown, while in Figure 4 the velocity magnitude contours are plotted. For all free stream velocities, these figures demonstrate that velocity shows a boundary layer type variation. The velocity increases with distance from the plate and approaches the free stream velocity at the edge of boundary layer. The exact solution for the boundary layer thickness for water is given by the Blasius solution [26] which is equal to $\delta = 5(\nu x/U)^{1/2}$. That is, the boundary layer thickness decreases with the increase of free stream velocity and increases with the increase of effective kinematic viscosity. These trends are observed from Figures 3 and 4 for the nanofluids as well as water.

Careful examination of Figure 3b shows that the velocity profile across the vertical centreline of flat plate increases slightly as nanotube weight percentage increases. This is because the effective viscosity of nanofluid increases with increase of the weight percentage of FMWCNT, and the velocity profile becomes fuller. Similar observation can also be made from the contour plots presented in Figure 4.

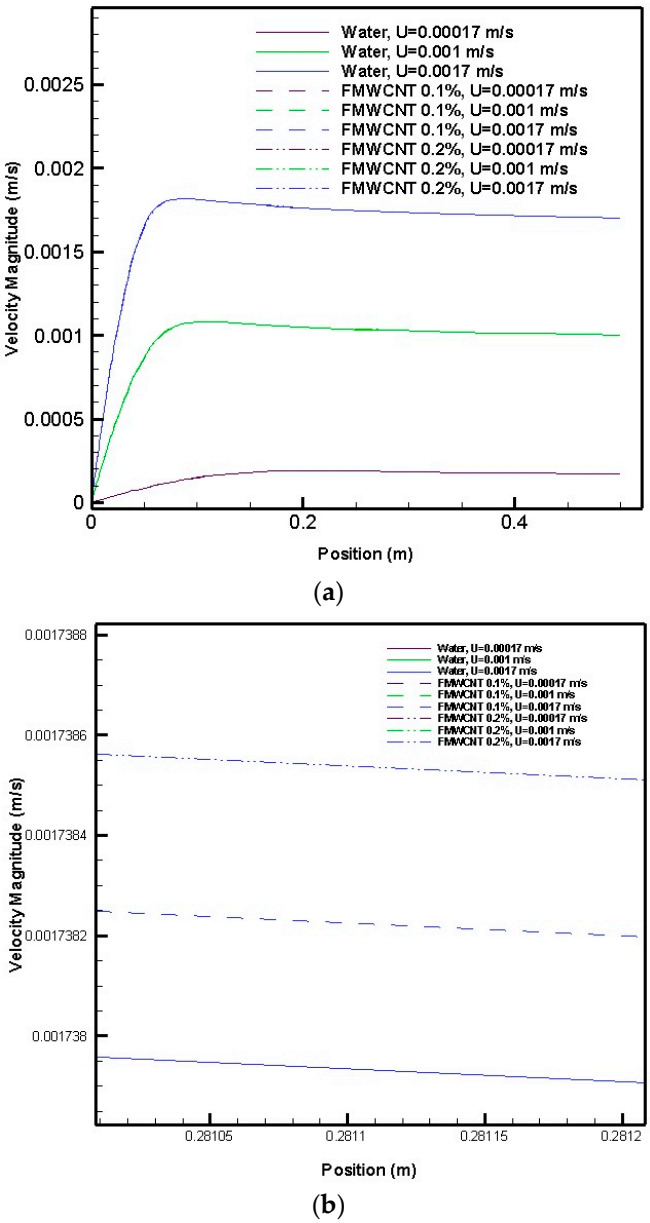

Figure 3. Velocity profiles versus distance from the plate at x = 0.5 m. (**a**) Full profile; (**b**) Enlarged segment near the plate.

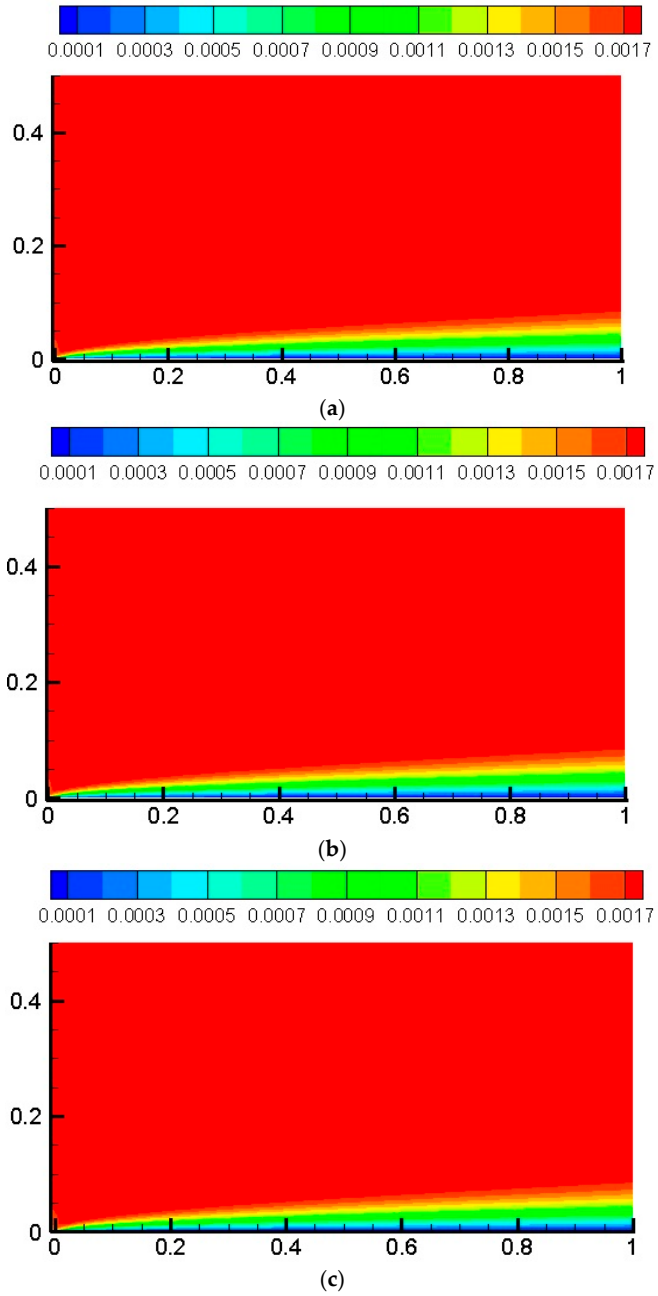

Figure 4. Contours of velocity magnitude for U = 0.0017 m/s and different nanofluids. (**a**) Distilled water; (**b**) ϕ = 0.1 wt. % MWCNT; (**c**) ϕ = 0.2 wt. % MWCNT.

Figure 5 shows the variations of wall shear stress for the range of studied parameters. For all cases, the wall shear stress value is high at the flat plate leading edge and decreases towards the outlet. The wall shear stress drops sharply in the beginning and continues to decrease with a much lower slope at distance from leading edge. It can be seen from the figure that, for a given free stream velocity, the wall shear stress values remain roughly the same for different solid weight percentages with concentration less or equal to 0.2%. This is due to the fact that, by increasing the nanotube weight percentage, the mixture viscosity increases. However, for low concentrations of FMWCNT, the increase is very small. For a constant nanotube weight percentage, however, the wall shear stress increases as the free stream velocity increases. The minimum and maximum of wall shear stress happen for U = 0.00017 m/s and U = 0.0017 m/s, respectively.

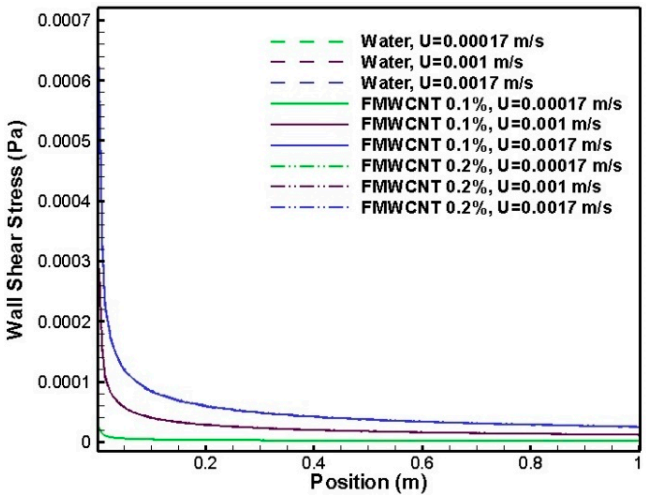

Figure 5. Wall shear stress variation along the flat plate.

The variation of Nusselt number along the flat plate for different cases is plotted in Figure 6. It is seen that the Nusselt number starts from its maximum value at the inlet and decreases asymptotically along the plate. The surface Nusselt number increases with free stream velocities and as the nanotube weight percentage increases. The Nusselt number is quite large in the entrance region because the boundary layer is thin and the temperature gradient is high near the wall.

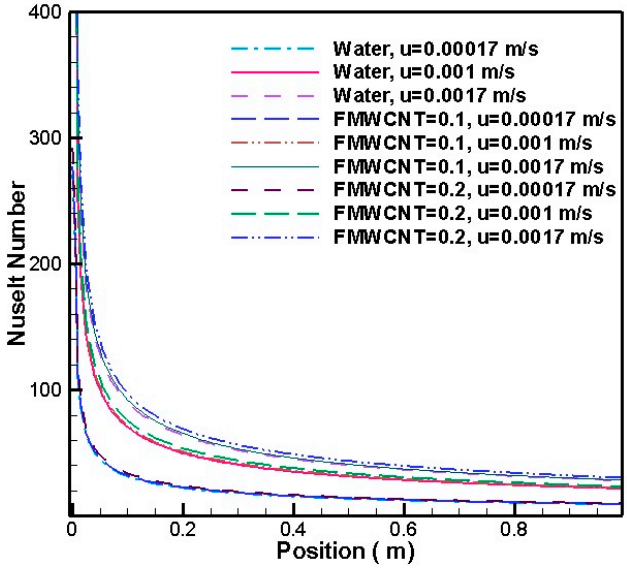

Figure 6. Nusselt number variation along the flat plate.

The temperature contours for different free stream velocities and nanotube weight percentages are presented in Figure 7. The development of the thermal boundary layer can also be clearly seen from this figure. As expected, the thermal boundary layer grows proportional to $X^{1/2}$. It is also seen that as the free stream velocity decreases or solid weight percentage increase, the thermal boundary layer thickness increase. However, the variation of the thermal boundary layer thickness with changes in the free stream velocities is more significant when compared with those for the nanotube weight percentages for concentrations of less or equal 0.2 percent.

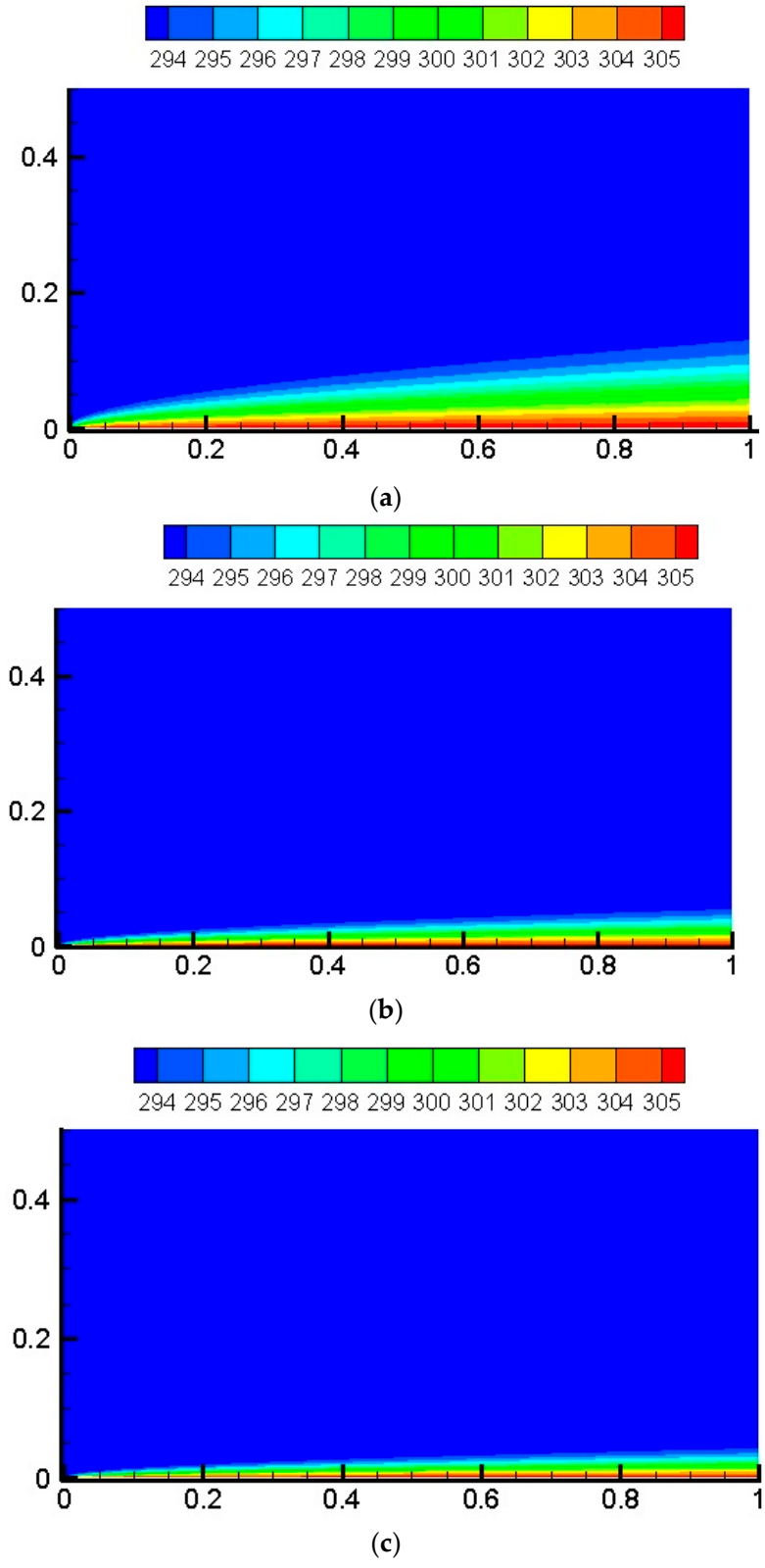

Figure 7. *Cont.*

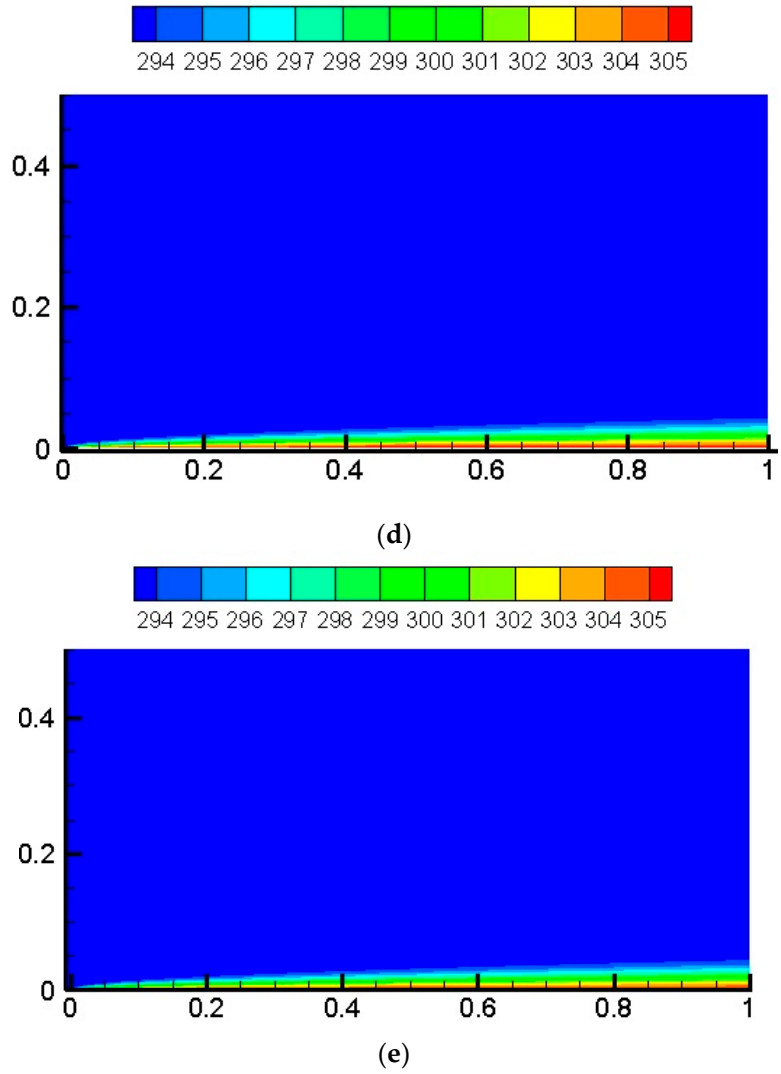

Figure 7. Temperature Contours of for different nanofluids and inlet velocities. (**a**) Distilled water, U = 0.00017 m/s; (**b**) Distilled water, U = 0.001 m/s; (**c**) Distilled water, U = 0.0017 m/s; (**d**) ϕ = 0.1 wt. % MWCNT, U = 0.0017 m/s; (**e**) ϕ = 0.2 wt. % MWCNT, U = 0.0017 m/s.

9. Conclusions

A numerical study of laminar forced convection heat transfer of water-based/functionalized multi-walled carbon nanotube (FMWCNT) nanofluid over a flat plate was presented. The nanofluid was simulated as a single-phase fluid mixture. The thermophysical properties of the nanofluid were obtained from the available experimental data reported in the literature. Different solid weight percentages and flow velocities were considered. The flow and temperature fields, as well as wall shear stress and Nusselt number were evaluated and discussed.

The significant observations made on the present study are summarized as follows:

(1) The Nusselt number of a nanofluid is augmented by increasing the weight percentage of nanotubes and the free stream velocity.
(2) For the range of concentration less than 0.2% FMWCNT, the effect of the nanotube weight percentage on wall shear stress is insignificant.
(3) Under similar conditions, the boundary layer thickness increases as free stream velocity decreases or particle volume fraction increases.

It should be pointed out there has been applications of two-fluid mixture [27,28] and even Eulerian-Lagrangian [29] models for analyzing nanofluids and accounting for the variation of the nanotube concentration in the domain. However, applications of these approaches to FMWCNT/water nanofluids are left for future studies.

Acknowledgments: The first and last authors would like to thank High Impact Research Grant UM.C/HIR/MOHE/ENG/45, UMRG Grant RP012D-13AET, and University of Malaya, Malaysia for their support in conducting this research work. A brief earlier version of this paper was presented at the Second National Conference of Application Researches in Electrical, Mechanical and Mechatronics, Tehran, Iran, 2015.

Author Contributions: The numerical part and coding have been done by Mohammad Reza Safaei and Mohammad Shahab Goodarzi. The data has been analyzed by Goodarz Ahmadi and Mohammad Shahab Goodarzi. The manuscript has been written through the contributions of Goodarz Ahmadi, S.N. Kazi and Amin Kamyar. All authors read and approved the final manuscript.

Conflicts of Interest: The authors declare no conflict of interest. The founding sponsors had no role in the design of the study; in the collection, analyses, or interpretation of data; in the writing of the manuscript, and in the decision to publish the results.

Nomenclature

T	temperature (K)
k	thermal conductivity ($W \cdot m^{-2} \cdot K^{-1}$)
t	time (s)
P	pressure (Pa)
C_p	specific heat capacity ($J \cdot kg^{-1} \cdot K^{-1}$)
u, v	Velocity components ($m \cdot s^{-1}$)
Greek Symbols	
δ	Boundary layer thickness (m)
ρ	Density ($kg \cdot m^{-3}$)
μ	Dynamic viscosity (Pa·s)
υ	Kinematic viscosity ($m^2 \cdot s^{-1}$)
φ	Weight percentage of nanotubes
Subscripts	
Bf	Base fluid
nf	Nanofluid
∞	Infinity

References

1. Hassan, M.; Sadri, R.; Ahmadi, G.; Dahari, M.B.; Kazi, S.N.; Safaei, M.R.; Sadeghinezhad, E. Numerical Study of Entropy Generation in a Flowing Nanofluid Used in Micro-and Minichannels. *Entropy* **2013**, *15*, 144–155. [CrossRef]
2. Asadian, A.M.; Abouali, O.; Yaghoubi, M.; Ahmadi, G. The Effect of Temperature Dependent Electrical Conductivity on the MHD Natural Convection of Al_2O_3–Water Nanofluid in a Rectangular Enclosure. In Proceedings of the ASME 2014 12th International Conference on Nanochannels, Microchannels and Minichannels, Chicago, IL, USA, 3–7 August 2014.
3. Herwig, H.; Hausner, O. Critical view on "new results in micro-fluid mechanics": An example. *Int. J. Heat Mass Transf.* **2003**, *46*, 935–937. [CrossRef]
4. Goodarzi, M.; Safaei, M.R.; Vafai, K.; Ahmadi, G.; Dahari, M.; Kazi, S.N.; Jomhari, N. Investigation of nanofluid mixed convection in a shallow cavity using a two-phase mixture model. *Int. J. Therm. Sci.* **2014**, *75*, 204–220. [CrossRef]
5. Yarmand, H.; Ahmadi, G.; Gharehkhani, S.; Kazi, S.N.; Safaei, M.R.; Alehashem, M.S.; Mahat, A.B. Entropy generation during turbulent flow of zirconia-water and other nanofluids in a square cross section tube with a constant heat flux. *Entropy* **2014**, *16*, 6116–6132. [CrossRef]

6. Goshayeshi, H.R.; Goodarzi, M.; Safaei, M.R.; Dahari, M. Experimental study on the effect of inclination angle on heat transfer enhancement of a ferrofluid in a closed loop oscillating heat pipe under magnetic field. *Exp. Therm. Fluid Sci.* **2016**, *74*, 265–270. [CrossRef]
7. Safaei, M.R.; Ahmadi, G.; Goodarzi, M.S.; Safdari Shadloo, M.; Goshayeshi, H.R.; Dahari, M. Heat Transfer and Pressure Drop in Fully Developed Turbulent Flows of Graphene Nanoplatelets–Silver/Water Nanofluids. *Fluids* **2016**, *1*, 20. [CrossRef]
8. Malvandi, A.; Ganji, D.D.; Hedayati, F.; Yousefi Rad, E. An analytical study on entropy generation of nanofluids over a flat plate. *Alex. Eng. J.* **2013**, *52*, 595–604. [CrossRef]
9. Ahmad, S.; Pop, I. Mixed convection boundary layer flow from a vertical flat plate embedded in a porous medium filled with nanofluids. *Int. Commun. Heat Mass Transf.* **2010**, *37*, 987–991. [CrossRef]
10. Hamad, M.A.A.; Pop, I.; Md Ismail, A.I. Magnetic field effects on free convection flow of a nanofluid past a vertical semi-infinite flat plate. *Nonlinear Anal. Real World Appl.* **2011**, *12*, 1338–1346. [CrossRef]
11. Malvandi, A.; Hedayati, F.; Ganji, D.D. Slip effects on unsteady stagnation point flow of a nanofluid over a stretching sheet. *Powder Technol.* **2014**, *253*, 377–384. [CrossRef]
12. Safaei, M.R.; Gooarzi, M.; Akbari, O.A.; Shadloo, M.S.; Dahari, M. Performance Evaluation of Nanofluids in an Inclined Ribbed Microchannel for Electronic Cooling Applications. Available online: http://www.intechopen.com/books/electronics-cooling/performance-evaluation-of-nanofluids-in-an-inclined-ribbed-microchannel-for-electronic-cooling-appli (accessed on 20 September 2016).
13. Bejan, A. *Convection Heat Transfer*; John Wiley & Sons: Hoboken, NJ, USA, 2013; Volume 4.
14. Aboulhasan Alavi, S.M.; Safaei, M.R.; Mahian, O.; Goodarzi, M.; Yarmand, H.; Dahari, M.; Wongwises, S. A Hybrid Finite-Element/Finite-Difference Scheme for Solving the 3-D Energy Equation in Transient Nonisothermal Fluid Flow over a Staggered Tube Bank. *Numer. Heat Transf. Part B Fundam.* **2015**, *68*, 169–183. [CrossRef]
15. Goodarzi, M.; Safaei, M.R.; Karimipour, A.; Hooman, K.; Dahari, M.; Kazi, S.N.; Sadeghinezhad, E. Comparison of the finite volume and lattice boltzmann methods for solving natural convection heat transfer problems inside cavities and enclosures. *Abstr. Appl. Anal.* **2014**, *2014*, 762184. [CrossRef]
16. Nikkhah, Z.; Karimipour, A.; Safaei, M.R.; Forghani-Tehrani, P.; Goodarzi, M.; Dahari, M.; Wongwises, S. Forced convective heat transfer of water/functionalized multi-walled carbon nanotube nanofluids in a microchannel with oscillating heat flux and slip boundary condition. *Int. Commun. Heat Mass Transf.* **2015**, *68*, 69–77. [CrossRef]
17. Amrollahi, A.; Rashidi, A.M.; Lotfi, R.; Emami Meibodi, M.; Kashefi, K. Convection heat transfer of functionalized MWNT in aqueous fluids in laminar and turbulent flow at the entrance region. *Int. Commun. Heat Mass Transf.* **2010**, *37*, 717–723. [CrossRef]
18. Safaei, M.R.; Togun, H.; Vafai, K.; Kazi, S.; Badarudin, A. Investigation of heat transfer enhancement in a forward-facing contracting channel using FMWCNT nanofluids. *Numer. Heat Transf. Part A* **2014**, *66*, 1321–1340. [CrossRef]
19. Wasistho, B.; Geurts, B.; Kuerten, J. Simulation techniques for spatially evolving instabilities in compressible flow over a flat plate. *Comput. Fluids* **1997**, *26*, 713–739. [CrossRef]
20. Patankar, S.V. *Numerical heat transfer and fluid flow, Series in Computational Methods in Mechanics and Thermal Sciences*; Hemisphere Publishing Corporation: Washington, DC, USA, 1980.
21. Safaei, M.R.; Goodarzi, M.; Mohammadi, M. Numerical modeling of turbulence mixed convection heat transfer in air filled enclosures by finite volume method. *Int. J. Multiphys.* **2011**, *5*, 307–324. [CrossRef]
22. Rahmanian, B.; Safaei, M.R.; Kazi, S.N.; Ahmadi, G.; Oztop, H.F.; Vafai, K. Investigation of pollutant reduction by simulation of turbulent non-premixed pulverized coal combustion. *Appl. Therm. Eng.* **2014**, *73*, 1222–1235. [CrossRef]
23. Togun, H.; Ahmadi, G.; Abdulrazzaq, T.; Shkarah, A.J.; Kazi, S.; Badarudin, A.; Safaei, M. Thermal performance of nanofluid in ducts with double forward-facing steps. *J. Taiwan Inst. Chem. Eng.* **2015**, *47*, 28–42. [CrossRef]
24. Karimipour, A.; Afrand, M.; Akbari, M.; Safaei, M.R. Simulation of Fluid Flow and Heat Transfer in the Inclined Enclosure. *Int. J. Mech. Aerosp. Eng.* **2012**, *6*, 86–91.
25. Schlichting, H. *Boundary-Layer Theory*; McGraw-Hill: New York, NY, USA, 1968.
26. White, F.M.; Corfield, I. *Viscous Fluid Flow*; McGraw-Hill: New York, NY, USA, 2006; Volume 3.

27. Ahmadi, G. On mechanics of saturated granular materials. *Int. J. Non-Linear Mech.* **1980**, *15*, 251–262. [CrossRef]
28. Ahmadi, G. On the mechanics of incompressible multiphase suspensions. *Adv. Water Resour.* **1987**, *10*, 32–43. [CrossRef]
29. Safaei, M.R.; Mahian, O.; Garoosi, F.; Hooman, K.; Karimipour, A.; Kazi, S.N.; Gharehkhani, S. Investigation of Micro- and Nanosized Particle Erosion in a 90° Pipe Bend Using a Two-Phase Discrete Phase Model. *Sci. World J.* **2014**, *2014*, 740578. [CrossRef] [PubMed]